

ORIGINAL ARTICLE

Open Access



Compound Impedance Control of a Hydraulic Driven Parallel 3UPS/S Manipulator

Lihang Wang¹, Shaofei Cui¹, Chong Ma¹ and Lijie Zhang^{1,2*}

Abstract

The hydraulic parallel manipulator combines the high-power density of the hydraulic system and high rigidity of the parallel mechanism with excellent load-carrying capacity. However, the high-precision trajectory tracking control of the hydraulic parallel manipulator is challenged by the coupling dynamics of the parallel mechanism and the high nonlinearities of the hydraulic system. In this study, the trajectory control of a 3-DOF symmetric spherical parallel 3UPS/S manipulator is evaluated. Focusing on the highly coupling and nonlinear system dynamics, a compound impedance control method for a hydraulic driven parallel manipulator is proposed, which combines impedance control with the spatial motion characteristics of a parallel manipulator. The control strategy is divided into the inner and outer loops. The inner loop controls the impedance of the actuator in the joint space, and the outer loop controls the impedance of the entire platform in the task space to compensate the coupling of the actuators and improve the tracking accuracy of the moving platform. Compound impedance control does not require force or pressure sensors and is less dependent on modeling precision. The experimental results show that the compound impedance control effectively improves the tracking accuracy of the moving platform. This research proposes a compound impedance control strategy for a 3-DOF hydraulic parallel manipulator, which has high tracking precision with a simple and cheap system configuration.

Keywords: Parallel manipulator, Impedance control, Hydraulic servo system, Trajectory tracking

1 Introduction

Parallel manipulators are widely applied in flight simulators [1, 2], machine tools [3], and six-dimensional force sensors [4] because they have higher stiffness, increased precision, lower inertia of moving parts at a high speed, and higher accuracy than those of their serial counterparts. However, their closed chain structure creates a complicated forward kinematic analysis and highly coupled time-varying nonlinear system dynamics. In addition, the uncertainty in the manipulator parameters and disturbances make it difficult to achieve high trajectory tracking control for parallel manipulators.

A number of works have investigated improving the tracking accuracy of parallel manipulators. PID control is the conventional and simplest method used to control the system and is widely used in parallel manipulators. However, because of the highly nonlinear and coupled dynamic behavior of parallel manipulators, the tracking error of pure PID control rapidly increases with speed [5]. To improve the performance of the PID controller, Amit Shukla proposed a novel controller that includes a PID controller and a compensator to deal with the coupling terms and varying parameters [6]. Londhe et al. [7] proposed a robust nonlinear PID-like fuzzy control scheme for a 3-DOF parallel manipulator, by combining a feed forward term and PID-like fuzzy logic control. However, these methods cannot achieve a high tracking accuracy.

To overcome the highly coupled dynamics of parallel manipulators, a number of model-based control methods

*Correspondence: ljzhang@ysu.edu.cn

¹ Hebei Key Laboratory of Heavy Machinery Fluid Power Transmission and Control, Yanshan University, Qinhuangdao 066004, China
Full list of author information is available at the end of the article

have been proposed, such as computed torque control [8, 9], feedforward force with PD feedback control [10, 11], adaptive control [12, 13], and robust control [14, 15]. A computed torque controller has been proposed for parallel manipulators, which is well suited for trajectory tracking control and disturbance rejection. However, the computed torque controller depends on the knowledge of the system, and the performance is generally significantly degraded when the modeling is inaccurate. Tien Dung Le proposed an online self-gain tuning method for a 2-DOF planar parallel manipulator, which is based on a combination of a conventional computed torque controller and an online tuning method using the neural network [16]. Feedforward force with PD feedback control is a popular control strategy applied to parallel manipulators. This method combines the advantages of calculated torque control and PID control and reduces the dependence of the calculated torque control on the accuracy of the system model. To reduce the dynamic tracking error in a highly real time application, Yang et al. [17] proposed a computed force and velocity controller for hydraulic 6-DOF parallel manipulators, which is composed of a conventional PID feedback controller and a desired driven force and actuator velocity as feed forward.

The adaptive control method enhances the adaptability of the control performance for the uncertainty by constructing a new dynamic system to continuously learn the system characteristics. Considering the uncertainty effect caused by a combination of rigid body parameters, friction, and actuator dynamics, Casalilla et al. [18] developed an adaptive controller for trajectory tracking control of a 3-DOF parallel manipulator. The application of adaptive control in parallel mechanisms reduces the requirement of precise dynamic modeling in the controller. However, the adaptive control increases the real-time calculation burden of the controller, and the realization of adaptive control requires meeting the persistence excitation conditions, which improves the requirements of the tracking trajectory. Robust control can also deal with model uncertainties. Li et al. [19] designed a controller based on a passivity-based robust control scheme for a 3-PRC parallel manipulator. Other robust control methods include linear robust control [20], sliding mode control [21], etc.; however, the common disadvantage of these methods is that it leads to a chattering problem, which significantly reduces trajectory tracking performance.

Impedance control [22] improves the motion of the manipulators by adjusting the relationship between the motion and driving force. It is typically used in applications that require complex interaction with the environment, such as assembly, drilling, and milling. However, some researches [23, 24] have shown that impedance

control also demonstrates the desirable trajectory tracking ability in free motion. The tracking ability of impedance control in free motion can be explained by introducing the concept of a virtual surface. Ghosh [25] proposed a robust control framework based on a bond graph modeling process. This method reduces the influence of system dynamics parameter uncertainties by adding dominant terms for complex and highly non-linear robot dynamics. For manipulators with flexible foundations, Pathak et al. [26] improved the above method to eliminate the interference of flexible foundations more effectively without knowing the dynamic parameters of flexible foundations by adjusting the dynamic characteristics of the mechanism in the form of an algorithm. Based on the physical reliability of the flexible foundation, the virtual surface concept is further proposed. The impedance controller constructs the virtual surface through the desired trajectory in real time and realizes trajectory tracking in free motion by adjusting the motion error between the actual position and virtual surface; thus, trajectory tracking control is realized.

Recently, lower-mobility parallel mechanisms were widely used in aviation, medical, and other industries owing to the lower cost and simpler controller [27]. Considering joint couplings, Liu et al. [28] proposed an iterative approach for feedforward controller parameter tuning for a 3-DOF parallel mechanism. For a 2-DOF 2PRP-PPR parallel manipulator, Santhakumar Mohan [29] proposed a robust cascaded control scheme for the end-effector pose error correction in trajectory tracking caused by mechanical inaccuracies. Angel et al. [30] applied a computed torque control strategy with a fractional order PID method. This strategy shows a robust and active disturbance rejection compared to that with the integer order PID method. The research objective of this study is a 3-DOF spherical space parallel 3UPS/S mechanism for wave compensation, whose tracking accuracy affects the quality of compensation.

As an important driving form, hydraulic actuators provide an attractive alternative for parallel manipulators, because they are robust and can produce significant forces/torques for their size without concern of overloading. However, the highly nonlinear dynamics and uncertainties in the hydraulic system make their closed-loop control design extremely challenging [31]. Common control strategies considering the dynamics of hydraulic actuators for parallel manipulators include cascade control [32, 33], backstepping control [34], virtual decomposition control [35], etc. One of the key problems in motion control of the hydraulic driven parallel mechanism is realizing high-precision driving force control of the hydraulic system. Guo et al. [33] integrated non-linear compensation of the flow rate of the servo valve,

positive velocity feedback, and load pressure feedback to control the pressure of the two chambers of the hydraulic cylinder. Considering the influence of the pipeline pressure transients and friction, Yang et al. [1] monitored the driving force in real time using a force sensor and obtained the piston force controller of the hydraulic actuator based on feedback linearization. Huang et al. [36] applied incremental nonlinear dynamic inversion (INDI) to design a robust force controller based on the pressure/force sensor and obtained better force tracking performance than that of the feedback linearization method. The control performance of the above methods depends on the high precision force/pressure sensor, which limits the application of these methods. Yoo et al. [37] presented an impedance control approach for a hydraulic system that required no external force/pressure sensors based on a backdrivable servovalve. However, the manufacturing cost of this type of system is relatively high.

In this paper, a compound impedance control method is proposed for a 3-DOF hydraulic parallel manipulator. The proposed method adopts a double loop structure to deal with the highly coupling dynamic and complex driving characteristics of hydraulic parallel manipulators. The proposed method does not require exact system dynamic parameters, such as mass distribution and friction. The proposed method uses a simplified asymmetric hydraulic servo system model based on a singular perturbation analysis, which has the characteristics of universality. Moreover, the proposed method uses the displacement sensors and regular servo-valves without expensive force or pressure sensors, creating a simple and cheap system configuration. The experimental result shows that the proposed method can track the typical reference signals according to wave motion and achieve a higher tracking accuracy than that of the fine-tuned PID controller.

The paper is organized as follows. The dynamic models of the 3UPS/S parallel mechanism and hydraulic actuator are established in the second and third section. In the fourth section, the singular perturbation analysis for the hydraulic servo system is discussed. The relationship between the input signal of the valve and the driving force is given, and the exponential convergence of the corresponding boundary layer model is determined. Then, the impedance control processes in the joint space and task space are described. Finally, the overall structure of the compound impedance control is given. In the fifth section, the 3UPS/S manipulator prototype is developed. Experiments are carried out for the tracking performance validation of the proposed method compared with the well-tuned PID control.

2 Modeling of the 3UPS/S Parallel Manipulator

As shown in Figure 1, the moving platform of 3UPS/S is connected to the fixed platform by a central spherical joint and three symmetrically distributed actuators. The upper end of each actuator is connected to the moving platform by a spherical joint, and the lower end is connected to the fixed platform by universal joints. The 3UPS/S mechanism is driven by hydraulic actuators, and the posture of the moving platform is adjusted by changing the length of the actuators. In contrast to the Stewart mechanism, the center spherical joint restrains the three-dimensional translation of the moving platform, retaining the three-dimensional rotation of the moving platform. Considering the workspace characteristics of the mechanism, the pitching and rolling motion of the moving platform are mainly used in practice.

2.1 Modeling of the 3UPS/S Parallel Manipulator

As shown in Figure 2, coordinate system $\{N\}$ is fixed to the fixed platform. Frame $\{A\}$ is fixed to the moving platform. The upper joint point distribution radius is R_1 . The joint point distribution radius is R_2 , and the center height of the central spherical joint is h .

The coordinates of the lower joint point B_i ($i = 1, 2, 3$) in $\{N\}$ can be expressed as

$$B_i(R_2 \cos \eta_i, R_2 \cos \eta_i, 0), \quad (1)$$

where $\eta_1 = \pi$, $\eta_2 = \pi/3$, $\eta_3 = -\pi/3$.

The coordinates of upper joint point A_i ($i = 1, 2, 3$) in $\{A\}$ can be expressed as follows:

$$A_i(R_1 \cos \eta_i, R_1 \cos \eta_i, 0). \quad (2)$$

The RPY angle is used to describe the relative motion relationship between the moving platform and fixed platform. The relationship between coordinate system $\{A\}$

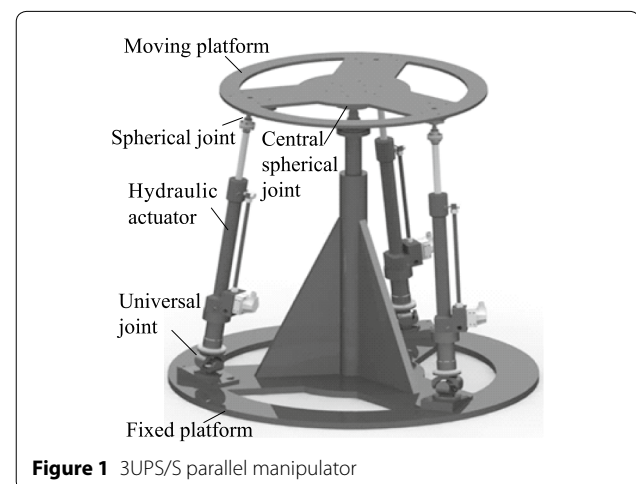


Figure 1 3UPS/S parallel manipulator

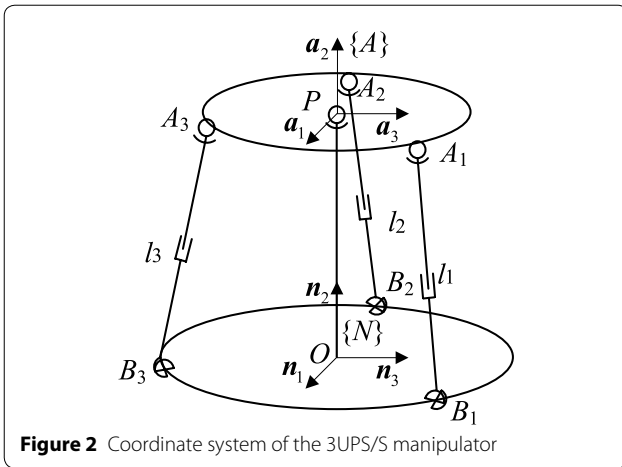


Figure 2 Coordinate system of the 3UPS/S manipulator

and coordinate system $\{N\}$ can be expressed by the rotation matrix.

$${}^N_A R = \begin{bmatrix} c_2 c_3 + s_1 s_2 s_3 & c_1 s_3 & s_1 c_2 s_3 - s_2 c_3 \\ s_1 s_2 c_3 - c_2 s_3 & c_1 s_3 & s_2 s_3 + s_1 c_2 c_3 \\ c_1 s_2 & -s_1 & c_1 c_2 \end{bmatrix}. \quad (3)$$

The transformation relationship between the vectors in $\{A\}$ and $\{N\}$ is as follows:

$${}^N \mathbf{u} = {}^A \mathbf{u}_A {}^N_A R, \quad (4)$$

where ${}^N \mathbf{u}$ and ${}^A \mathbf{u}$ represent the coordinates of vector \mathbf{u} in $\{A\}$ and $\{N\}$, respectively.

3UPS/S has three-dimensional rotational degrees of freedom around the central spherical joint, and the rotation angle of the moving platform relative to the fixed platform determines the posture of the manipulator. The length of the three actuators can be obtained uniquely from the rotation angle, which is referred to as the inverse kinematics model of the 3UPS/S manipulator.

$$l_i = |r^{A_i B_i}| = |r^{B_i O} + r^{OP} + r^{P A_i}|. \quad (5)$$

In $\{N\}$, the coordinates of each position vector are as follows.

$$\begin{aligned} {}^N r^{B_i O} &= -[R_2 \cos \eta_i, R_2 \cos \eta_i, 0], \\ {}^N r^{OP} &= [0, 0, h], \\ {}^N r^{P A_i} &= [R_1 \cos \eta_i, R_1 \cos \eta_i, 0] {}^N_A R. \end{aligned} \quad (6)$$

2.2 Inverse Dynamics Model

The dynamic model of the 3UPS/S parallel mechanism is established by Kane's method. The three-dimensional

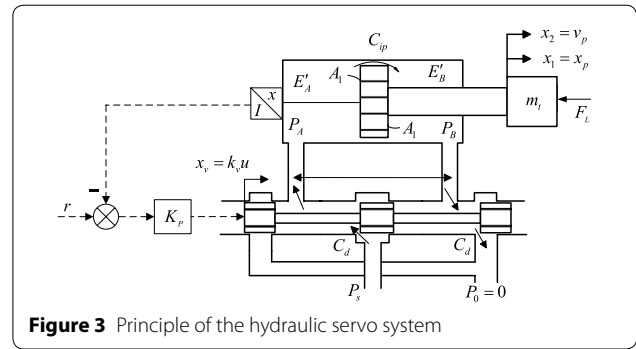


Figure 3 Principle of the hydraulic servo system

rotation in the task space of the moving platform is selected as the generalized coordinates and denoted as $\mathbf{q} = [q_1, q_2, q_3]^T$. The coordinate $\mathbf{u} = [u_1, u_2, u_3]^T$ of the angular velocity of the moving platform in $\{N\}$ is selected as the generalized velocity, which yields the following:

$$\boldsymbol{\omega}^A = u_1 \mathbf{n}_1 + u_2 \mathbf{n}_2 + u_3 \mathbf{n}_3. \quad (7)$$

The dynamics model of the 3UPS/S manipulator can be written as

$$\mathbf{T} + \mathbf{M}\mathbf{Q} + \mathbf{F}^* = \mathbf{0}, \quad (8)$$

where \mathbf{T} denotes the generalized active force caused by gravity and the forces in the Cartesian space of the moving platform, $\mathbf{T} = \mathbf{T}(\mathbf{q}, \mathbf{F}_L, \mathbf{T}_L, \mathbf{G})$; $\mathbf{F}_L, \mathbf{T}_L$ denotes the load force on the moving platform; \mathbf{M} denotes the mapping matrix of the driving force from the joint space to the workspace, $\mathbf{M} = \mathbf{M}(\mathbf{q})$; \mathbf{Q} denotes the driving force vector; \mathbf{F}^* denotes the generalized inertial force, $\mathbf{F}^* = \mathbf{F}^*(\mathbf{q}, \dot{\mathbf{q}}, \ddot{\mathbf{q}})$. The detailed expressions for the above symbols are given in Appendix.

The inverse dynamic model of 3UPS/S can be written as follows:

$$\mathbf{Q} = -\mathbf{M}^{-1}(\mathbf{T} + \mathbf{F}^*). \quad (9)$$

3 Dynamic Model of the Hydraulic Servo System

The 3UPS/S hydraulic servo system is shown in Figure 3, where r represents the input signal; K_p represents the proportional gain of the system; F_L represents the load force; P_s represents the supply pressure; P_0 represents the tank pressure; P_A and P_B represent the pressures of the two chambers of the hydraulic cylinder; A_1 and A_2 represent the effective area of the two chambers.

The bond graph model of the hydraulic servo system is shown in Figure 4, where R_f represents the friction of the hydraulic cylinder; $R_i (i = 1, 2, 3, 4)$ represents the four resistances of the servovalve.

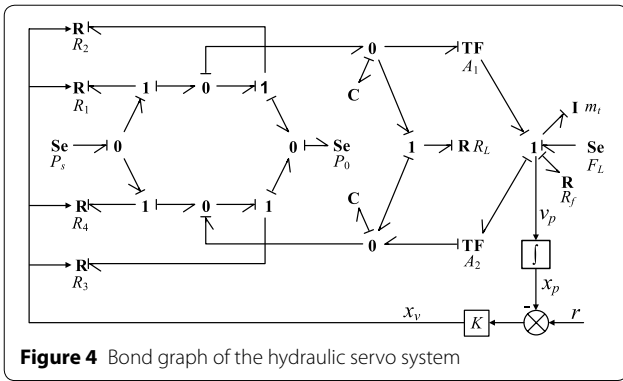


Figure 4 Bond graph of the hydraulic servo system

The servo valve can be expressed as four hydraulic resistances connected to each other, which can be expressed as follows:

$$\begin{aligned}
 Q_{PA} &\triangleq f_1(x_v, \Delta P_1) = \begin{cases} C_d w x_v \sqrt{\frac{2|\Delta P_1|}{\rho}}, & x_v > 0, \\ 0, & x_v \leq 0, \end{cases} \\
 Q_{AT} &\triangleq f_2(x_v, \Delta P_2) = \begin{cases} 0, & x_v > 0, \\ -C_d w x_v \sqrt{\frac{2|\Delta P_2|}{\rho}}, & x_v \leq 0, \end{cases} \\
 Q_{BT} &\triangleq f_3(x_v, \Delta P_3) = \begin{cases} C_d w x_v \sqrt{\frac{2|\Delta P_3|}{\rho}}, & x_v > 0, \\ 0, & x_v \leq 0, \end{cases} \\
 Q_{PB} &\triangleq f_4(x_v, \Delta P_4) = \begin{cases} 0, & x_v > 0, \\ -C_d w x_v \sqrt{\frac{2|\Delta P_4|}{\rho}}, & x_v \leq 0. \end{cases}
 \end{aligned} \tag{10}$$

Here, P , T , A , and B represent the four ports of the servo valve; Q_{PA} , Q_{AT} , Q_{BT} and Q_{PB} denote the flow of the corresponding valve port, which is in the positive direction of P to A , A to T , B to T , and P to B , respectively; C_d represents the flow coefficient of the valve orifice; w represents the gradient of the servo orifice area with the opening of the valve; x_v represents the displacement of the spool; ρ represents the density of the oil, and ΔP_i ($i = 1, 2, 3, 4$) represents the differential pressure between the corresponding ports.

$$\begin{aligned}
 \Delta P_1 &\triangleq P_s - P_A, \quad \Delta P_2 \triangleq P_A - P_0, \\
 \Delta P_3 &\triangleq P_B - P_0, \quad \Delta P_4 \triangleq P_s - P_B.
 \end{aligned} \tag{11}$$

The friction force of the hydraulic cylinder is assumed to be proportional to the velocity.

$$F_f = C v_p, \tag{12}$$

where C is the damping coefficient, and v_p is the velocity of the hydraulic actuator.

Assuming that the internal leakage of the hydraulic cylinder is small and can be ignored, the model of the hydraulic servo system can be expressed as follows:

$$\begin{cases} \dot{x}_1 = x_2, \\ \dot{x}_2 = \frac{1}{m_t} (A_1 x_3 - A_2 x_4 + F_L - C_v x_2), \\ \dot{x}_3 = \frac{E'_A}{V_A} [f_1(x_v, P_s - x_3) - f_2(x_v, x_3 - P_0) - x_2 A_1], \\ \dot{x}_4 = \frac{E'_B}{V_B} [f_4(x_v, P_s - x_4) - f_3(x_v, x_4 - P_0) + x_2 A_2]. \end{cases} \tag{13}$$

Assumption 1 In a practical hydraulic system under normal working conditions, P_1 and P_2 are bounded by P_0 and P_s , i.e., $P_0 \leq P_1, P_2 \leq P_s$.

4 Controller Design

4.1 Hydraulic Driving Force Model Based on Singular Perturbation

An important problem in a hydraulic driven parallel manipulator is the force generation in the hydraulic servo system. In this study, the relationship between the valve input signal and driving force is determined by a singular perturbation analysis. Most physical system models can be described by states with different rates, which can be divided into boundary layer subsystems described by faster states and reduced order subsystems described by slower states. The Tikhonov theorem [38] states that when the boundary layer model is stable, the fast-changing states can be removed, while the static relationship is considered the boundary condition to participate in the process of the slow-changing states, thus achieving system dimensionality reduction and simplification. The singular perturbation analysis is widely applied in the hydraulic servo system [39]. Based on the above analysis, the hydraulic servo system can be described by four states: the pressure states and mechanical states, which refer to the displacement and velocity of the actuator. Because of the pressure conduction characteristics of oil, the rate of the pressure states is much faster than that of the mechanical states. Through singular perturbation, the relationship between the valve input signal and driving force can be obtained from the static relation of the fast-changing states. In this section, the corresponding singular perturbation analysis process and the proof of the exponential convergence of the boundary layer are given.

For the hydraulic servo system described in Eq. (13), the mechanical state is $x_h = [x_1, x_2]^T$, and the pressure state of the hydraulic system is $z_h = [x_3, x_4]^T$.

Considering the difference between the bulk modulus of the two chambers, the following is assumed:

$$\frac{1}{E'_A} = \varepsilon, \quad \frac{1}{E'_B} = \frac{1}{kE'_A} = \frac{1}{k}\varepsilon. \tag{14}$$

The state equation for pressure can be written as follows:

$$\begin{aligned} \varepsilon \dot{x}_3 &= \frac{1}{V_A} [f_1 - f_2 - A_1 x_2], \\ \varepsilon \dot{x}_3 &= \frac{k}{V_B} [f_4 - f_3 - A_2 x_2]. \end{aligned} \tag{15}$$

Substituting Eq. (10) into Eq. (15) with $\varepsilon = 0$, a quasi-static representation of the pressure state is given by

$$h_1 \triangleq \bar{x}_3 = \begin{cases} P_s - \frac{A_1^2}{K_{Q1}^2} \cdot \frac{x_2^2}{u^2}, & u > 0, \\ P_0 + \frac{A_1^2}{K_{Q1}^2} \cdot \frac{x_2^2}{u^2}, & u < 0, \end{cases} \tag{16}$$

$$h_2 \triangleq \bar{x}_4 = \begin{cases} P_0 + \frac{A_2^2}{K_{Q2}^2} \cdot \frac{x_2^2}{u^2}, & u > 0, \\ P_s - \frac{A_2^2}{K_{Q2}^2} \cdot \frac{x_2^2}{u^2}, & u < 0, \end{cases}, \tag{17}$$

where $K_{Q1} \triangleq C_{d1} w_1 K_v \sqrt{\frac{\rho}{2}}$, $K_{Q2} \triangleq C_{d2} w_2 K_v \sqrt{\frac{\rho}{2}}$.

The simplified order reduction model of the hydraulic servo system can be obtained by substituting Eqs. (16) and (17) into Eq. (18):

$$\begin{cases} \dot{x}_1 = x_2, \\ \dot{x}_2 = \frac{1}{m_t} (A_1 h_1 - A_2 h_2 - C_v x_v + F_L). \end{cases} \tag{18}$$

The boundary layer model of the hydraulic servo system can be written as follows:

$$\begin{cases} \varepsilon \dot{x}_3 = \frac{1}{V_A} (f_1 - f_2 - A_1 x_2), \\ \varepsilon \dot{x}_4 = \frac{k}{V_B} (f_4 - f_3 + A_2 x_2). \end{cases} \tag{19}$$

The auxiliary variable $\mathbf{y} = \mathbf{z}_h - \mathbf{h}(t, \mathbf{x})$ is introduced to move the equilibrium point of the boundary layer model to the origin:

$$\begin{cases} y_1 = x_3 - h_1, \\ y_2 = x_4 - h_2. \end{cases} \tag{20}$$

Substituting Eq. (20) into Eq. (19) and introducing time variable $\tau = \frac{1}{\varepsilon}(t - t_0)$, the boundary layer model is given as follows:

$$\frac{dy_1}{d\tau} = \frac{1}{V_A} (f_1 - f_2 - A_1 x_2), \tag{21}$$

where

$$f_1 - f_2 = \begin{cases} K_{Q1} u \sqrt{P_s - (y_1 + h_1)}, & u > 0, \\ K_{Q1} u \sqrt{(y_1 + h_1) - P_0}, & u < 0. \end{cases} \tag{22}$$

When $u > 0$,

$$\begin{aligned} f_1 - f_2 &= K_{Q1} u \sqrt{P_s - \left(y_1 + P_s - \frac{A_1^2}{K_{Q1}^2} \frac{x_2^2}{u^2} \right)} \\ &= \sqrt{A_1^2 x_2^2 - y_1 u^2 K_{Q1}^2}. \end{aligned} \tag{23}$$

Based on Assumption 1, one can obtain the following:

$$A_1^2 x_2^2 - y_1 u^2 K_{Q1}^2 \geq 0. \tag{24}$$

When $u < 0$,

$$\begin{aligned} f_1 - f_2 &= K_{Q1} u \sqrt{\left(y_1 + P_0 + \frac{A_1^2}{K_{Q1}^2} \frac{x_2^2}{u^2} \right) - P_0} \\ &= -\sqrt{A_1^2 x_2^2 + y_1 u^2 K_{Q1}^2}. \end{aligned} \tag{25}$$

Based on Assumption 1, one can obtain the following:

$$A_1^2 x_2^2 + y_1 u^2 K_{Q1}^2 \geq 0. \tag{26}$$

The following boundary layer model is obtained:

$$\frac{dy_1}{d\tau} = \begin{cases} \frac{1}{V_A} \left(\sqrt{A_1^2 x_2^2 - y_1 u^2 K_{Q1}^2} - A_1 x_2 \right), & u > 0, \\ \frac{1}{V_A} \left(-\sqrt{A_1^2 x_2^2 + y_1 u^2 K_{Q1}^2} - A_1 x_2 \right), & u < 0. \end{cases} \tag{27}$$

When $u > 0, x_2 > 0, |x_2| = x_2$,

$$\frac{dy_1}{d\tau} = \frac{1}{V_A} \left(\sqrt{A_1^2 x_2^2 - y_1 u^2 K_{Q1}^2} - A_1 |x_2| \right). \tag{28}$$

When $u < 0, x_2 < 0, |x_2| = -x_2$,

$$\frac{dy_1}{d\tau} = \frac{1}{V_A} \left(A_1 |x_2| - \sqrt{A_1^2 x_2^2 + y_1 u^2 K_{Q1}^2} \right). \tag{29}$$

Here, $\mathbf{y} = 0$ is the equilibrium point of $\frac{dy}{d\tau} = \mathbf{g}$. After linearization, the stability of the boundary layer model is evaluated by solving the Jacobian matrix.

The Jacobian matrix can be written as follows:

$$\mathbf{J} = \frac{\partial \mathbf{g}}{\partial \mathbf{y}} = \begin{bmatrix} \frac{\partial g_1}{\partial y_1} & 0 \\ 0 & \frac{\partial g_2}{\partial y_2} \end{bmatrix}, \tag{30}$$

where

$$\frac{\partial g_1}{\partial y_1} = \begin{cases} -\frac{1}{V_A} \frac{u^2 K_{Q1}^2}{\sqrt{A_1^2 x_2^2 - y_1 u^2 K_{Q1}^2}}, & u > 0, \\ -\frac{1}{V_A} \frac{u^2 K_{Q1}^2}{\sqrt{A_1^2 x_2^2 + y_1 u^2 K_{Q1}^2}}, & u \leq 0. \end{cases} \quad (31)$$

With Eq. (24), the following is obtained:

$$A_1^2 x_2^2 \geq |y_1 u^2 K_{Q1}^2|, \quad (32)$$

then

$$\begin{aligned} |A_1^2 x_2^2 - y_1 u^2 K_{Q1}^2| &\leq |A_1^2 x_2^2| + |y_1 u^2 K_{Q1}^2| \leq 2|A_1^2 x_2^2|, \\ |A_1^2 x_2^2 + y_1 u^2 K_{Q1}^2| &\leq |A_1^2 x_2^2| + |y_1 u^2 K_{Q1}^2| \leq 2|A_1^2 x_2^2|. \end{aligned} \quad (33)$$

The sign of $\frac{\partial g_1}{\partial y_1}$ yields

$$\frac{\partial g_1}{\partial y_1} \leq -\frac{1}{V_A} \frac{u^2 K_{Q1}^2}{\sqrt{2A_1^2 x_2^2}} < 0. \quad (34)$$

Similarly, by defining $y_2 = z_2 - h_2 = x_4 - h_2$, the sign of $\frac{\partial g_2}{\partial y_2}$ is given by

$$\frac{\partial g_2}{\partial y_2} \leq -\frac{1}{V_B} \frac{u^2 K_{Q2}^2}{\sqrt{2A_2^2 x_2^2}} < 0. \quad (35)$$

The boundary layer model satisfies $\text{Re} \left[\lambda \left\{ \frac{\partial g}{\partial y} \right\} \right] \leq -c < 0, \forall (t, x) \in [0, t_1] \times D_x$. Thus, the boundary layer model of the singularly perturbed system has exponential convergence [38].

4.2 Hydraulic Driving Force Model Based on Singular Perturbation

The relationship between the valve input signal and output force of the hydraulic cylinder piston is obtained by the singular perturbation analysis for the hydraulic servo system. To realize position tracking control, the relationship between the output force and motion of the hydraulic actuator should be determined. To achieve an effective and stable drive, this relationship is designed as a spring damping model, as shown in Figure 5.

The desired force F_v satisfies

$$F_v \triangleq -K_1(x_1 - r) - K_2(x_2 - \dot{r}). \quad (36)$$

With the singular perturbation analysis, by ignoring the tank pressure, the driving force yields

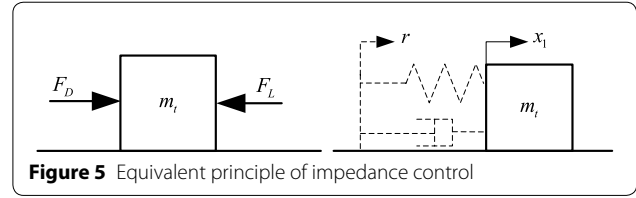


Figure 5 Equivalent principle of impedance control

$$F_D = \begin{cases} A_1 P_s - K_A \frac{x_2^2}{u^2}, & u > 0, \\ -\left(A_2 P_s - K_A \frac{x_2^2}{u^2} \right), & u < 0, \end{cases} \quad (37)$$

where K_A denotes the valve characteristic coefficient and is defined as follows:

$$K_A \triangleq \frac{A_1^3}{K_{Q1}^2} + \frac{A_1^3}{K_{Q2}^2}. \quad (38)$$

To realize trajectory tracking control, the following should be satisfied:

$$F_D - F_L = F_v = -K_1(x_1 - r) - K_2(x_2 - \dot{r}). \quad (39)$$

Here, F_L denotes the total load force, including the friction force.

After replacing the actual speed with the instruction speed, the final control law is obtained:

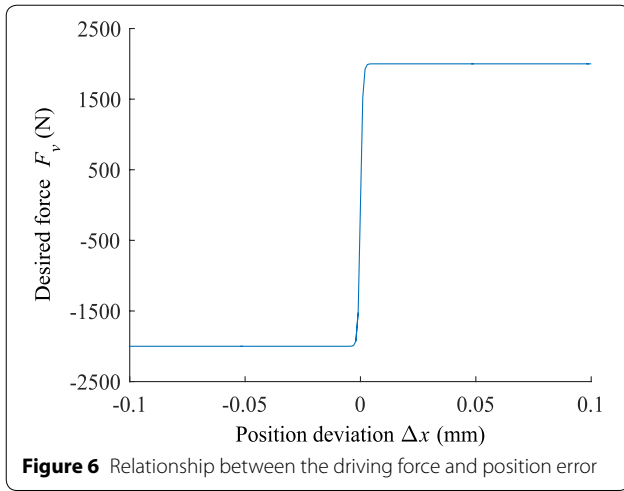
$$u = \begin{cases} |\dot{r}| \sqrt{\frac{K_A}{A_1 P_s - K_1 |r - x_1| + K_2 (x_2 - \dot{r}) - F_{L\max}}}}, & (r - x_1) > 0, \\ -|\dot{r}| \sqrt{\frac{K_A}{A_2 P_s - K_1 |r - x_1| + K_2 (x_2 - \dot{r}) - F_{L\max}}}}, & (r - x_1) < 0. \end{cases} \quad (40)$$

Remark 1 One of the advantages of this algorithm is that the stiffness expression can be freely programmed. The drive stiffness should be large enough to guarantee position accuracy and robustness. In addition, the output signal is required to be bounded without an infinite signal.

The drive stiffness could be planned by a hyperbolic tangent function, as shown in Figure 6.

$$F_D^S = \frac{F_m [1 + \tanh(k(r - x_1))] + F_m [\tanh(k(r - x_1)) - 1]}{2}. \quad (41)$$

Here, F_D^S denotes the driving force produced by the spring effect, and F_m is the maximum of the spring force.



Remark 2 To prevent output u from being infinite, the following should be satisfied:

$$\begin{aligned} A_1 P_s + F_D^S + K_2(x_2 - \dot{r}) - F_{Lmax}^* &> 0, \\ A_2 P_s + F_D^S + K_2(x_2 - \dot{r}) - F_{Lmax}^* &> 0. \end{aligned} \quad (42)$$

To improve system reliability, the output can be further limited:

$$\sqrt{\frac{K_A}{A_2 P_s + F_D^S + K_2(x_2 - \dot{r}) - F_{Lmax}^*}} \leq \frac{S_m}{|\dot{r}_0|}, \quad (43)$$

where S_m is the maximum input of the valve; \dot{r}_0 is a typical value of the command rate.

To track the abnormal reference speed, the effective command rate of 0.1–0.5 is used, substituting $\min(0.5, \max(|\dot{r}|, 0.1))$ for $|\dot{r}|$ in Eq. (40).

4.3 Impedance Control in the Task Space

The proposed impedance control is an operation process that takes load, command, and feedback signal as the input and the valve input signal as the output. To ensure reliability of the control process, the trajectory command of each actuator is obtained by an inverse kinematics model. Based on the idea of impedance control, the correcting moment is obtained from the motion deviation in the task space of the manipulator and then mapped to the additional driving force of each driving branch as the load input to compensate the overall motion characteristics of the manipulator.

When the manipulator is subjected to external torque T_s , the driving force in the equilibrium state is correspondingly increased by ΔQ . To obtain the mapping

relationship between external torque T_s and driving force increment ΔQ , the platform dynamic inverse model Eq. (9) is written in increment form:

$$\Delta Q = -M^{-1}(\Delta T), \quad (44)$$

where the external moment ΔT yields:

$$\Delta T = T_s \triangleq (T_x, T_y, T_z) \begin{bmatrix} \mathbf{n}_1 \\ \mathbf{n}_2 \\ \mathbf{n}_3 \end{bmatrix}. \quad (45)$$

Using Eqs. (44) and (45), the relationship between ΔT and ΔQ is given as follows:

$$\begin{bmatrix} \Delta Q_1 \\ \Delta Q_2 \\ \Delta Q_3 \end{bmatrix} = M^{-1} \begin{bmatrix} \Delta T \cdot \omega_1^A \\ \Delta T \cdot \omega_2^A \\ \Delta T \cdot \omega_3^A \end{bmatrix}. \quad (46)$$

The generalized velocity of the moving platform relative to the fixed platform yields the following:

$$\begin{aligned} {}^N \omega_1^A &= (1, 0, 0) \begin{bmatrix} \mathbf{n}_1 \\ \mathbf{n}_2 \\ \mathbf{n}_3 \end{bmatrix}, \quad {}^N \omega_2^A = (0, 1, 0) \begin{bmatrix} \mathbf{n}_1 \\ \mathbf{n}_2 \\ \mathbf{n}_3 \end{bmatrix}, \\ {}^N \omega_3^A &= (0, 0, 1) \begin{bmatrix} \mathbf{n}_1 \\ \mathbf{n}_2 \\ \mathbf{n}_3 \end{bmatrix}. \end{aligned} \quad (47)$$

The mapping relationship between the task space and joint space of the 3UPS/S manipulator yields the following:

$$\begin{bmatrix} Q_1 \\ Q_2 \\ Q_3 \end{bmatrix} = M^{-1} \begin{bmatrix} T_x \\ T_y \\ T_z \end{bmatrix}. \quad (48)$$

For impedance control, virtual spring damping is constructed in the task space, and the force is mapped to each actuator through matrix M^{-1} :

$$\Delta Q = -M^{-1}(K \Delta q + C \Delta \dot{q}). \quad (49)$$

4.4 Impedance Control in the Task Space

Compound impedance control performs impedance control in the joint space and task space. First, through the singular perturbation analysis of the hydraulic servo system, a single cylinder trajectory tracking control method, including load factors, is obtained and combined with impedance control. Then, for impedance control, virtual spring damping is constructed in the task space of the mechanism, and the force is mapped to the driving branch in reverse. For each actuator, trajectory tracking control is performed in the joint space of the manipulator,

and real-time adjustment is performed according to the motion error in the task space.

Combining the impedance control algorithm in the joint space, an additional driving force ΔQ_i is added to each actuator. The 3UPS/S overall control algorithm can be expressed as follows:

$$u = \frac{1 + \tanh(k(r - x_1 + h_v))}{2} u_i^+ + \frac{\tanh(k(r - x_1 + h_v)) - 1}{2} u_i^-, \tag{50}$$

where

$$u_i^+ \triangleq |\dot{r}| \sqrt{\frac{K_A}{A_1 P_s - K_1(r - x_1) - K_2(\dot{r} - x_2) - \Delta Q_i - F_{Lmax}}},$$

$$u_i^- \triangleq -|\dot{r}| \sqrt{\frac{K_A}{A_2 P_s + K_1(r - x_1) + K_2(\dot{r} - x_2) + \Delta Q_i - F_{Lmax}}}. \tag{51}$$

The corresponding block diagram is shown in Figure 7.

To realize the impedance control in the task space, the three-axis rotation angle should be obtained in the task space of the parallel platform in real time. Considering the measurement accuracy and reliability, an indirect measurement method is adopted to obtain the moving platform rotation angle by detecting the displacement of the driving joint based on forward kinematics solution of the manipulator. The forward kinematics analysis process of the 3UPS/S mechanism (nonlinear algebraic equations) is complex and has multiple solutions. In practice, numerical methods [40] are often applied to obtain the motion of the moving platform. In this study, the forward position solution of 3UPS/S is obtained using the neural network method, based on the comparison of accuracy and computational efficiency.

5 Prototype System and Experimental Results

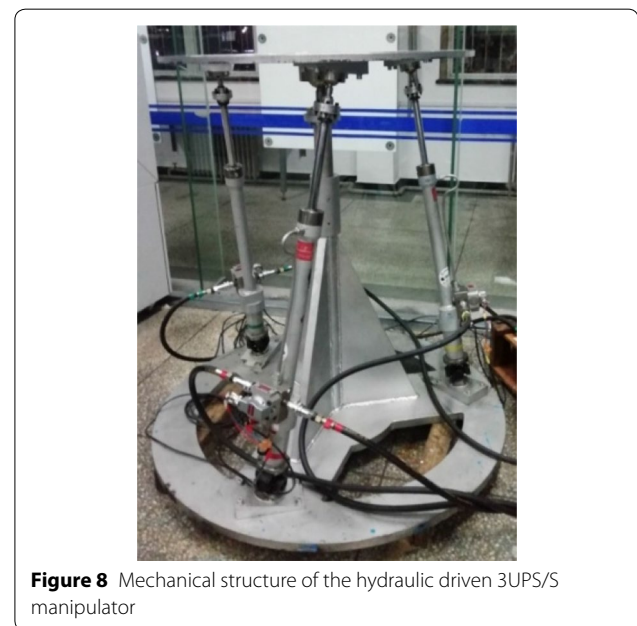
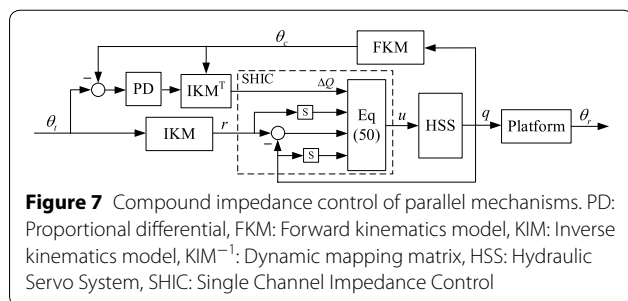
To verify the trajectory tracking performance of compound impedance control, a hydraulic driven 3UPS/S parallel manipulator prototype is developed, as shown

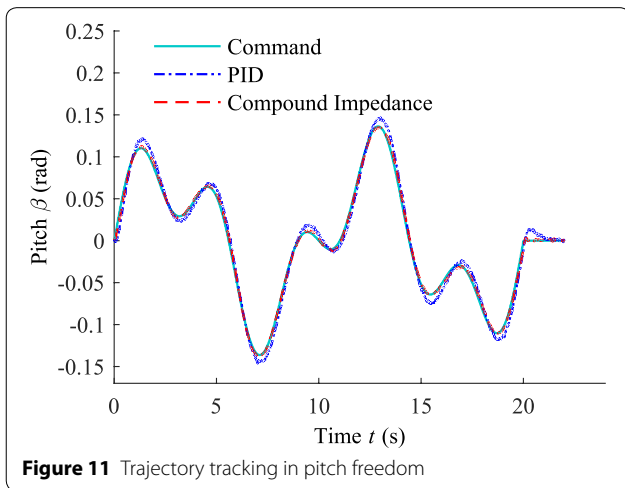
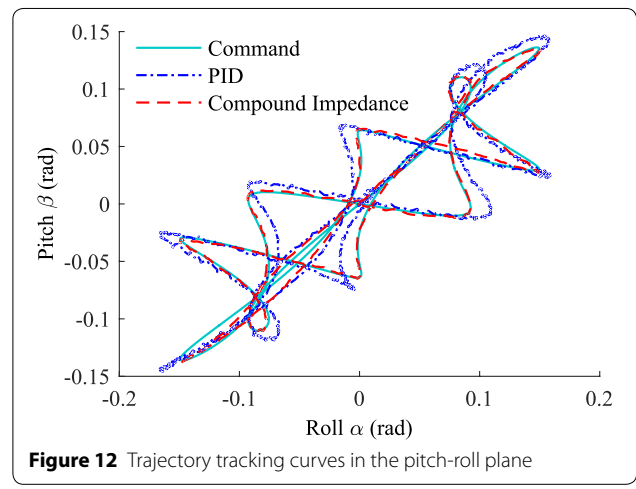
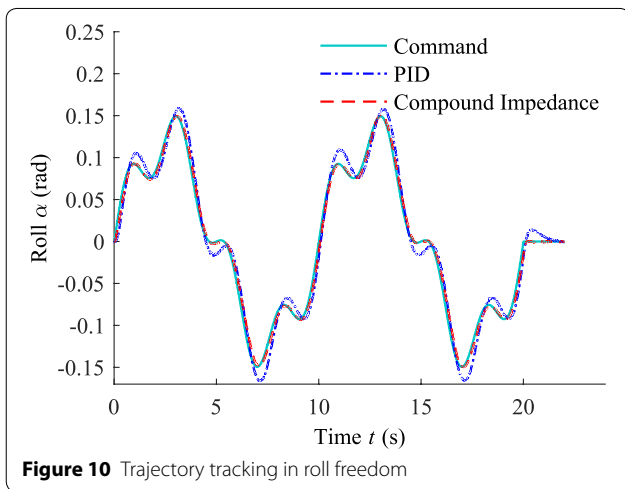
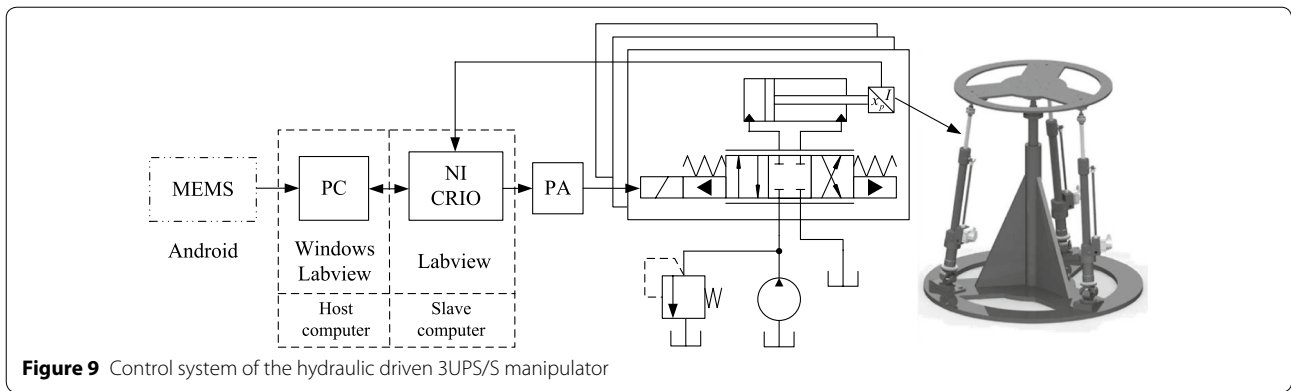
in Figure 8 and Figure 9. The control system consists of the host computer and slave computer. The host computer is implemented by Labview in Windows to realize command generation/reception, data supervision, and recording. The slave computer adopts the NI-cRIO controller and completes the trajectory tracking control of each actuator according to the sequence of the displacement command sent by the host computer. For the 3UPS/S manipulator prototype, the distribution radius is 0.38 m; the distribution radius of the joint point of the lower platform is 0.51 m; the height of the platform at the center of central ball joint h is 1.15 m; the initial

rotation angle of the moving platform is $\pi/6$; the stroke of the hydraulic actuator is 450 mm; the diameter of the hydraulic cylinder is 40 mm; the diameter of the hydraulic piston rod is 25 mm; the hydraulic cylinder displacement sensor accuracy is 0.02%, and the moving platform inclination sensor accuracy is $\pm 1.67 \times 10^{-3}$ rad. From the wave spectrum, the desired trajectories in two freedoms are designed as follows:

$$y_r = 0.1222 \sin(0.1 \cdot 2\pi t) + 0.03487 \sin(0.4 \cdot 2\pi t),$$

$$y_p = 0.0873 \sin(0.1 \cdot 2\pi t) + 0.05234 \sin(0.25 \cdot 2\pi t).$$





The platform is designed to compensate wave motion and provide a stable working environment for shipboard equipment. The tracking curves of the PID control and

compound impedance control for compound sinusoidal instructions with a frequency of 0.1–0.4 Hz, according to the statistical law of wave motion, are shown in Figure 10 and Figure 11. The classical PID control scheme is also applied to the parallel manipulator as a benchmark. For convenience of description, the rotation of the 3UPS/S platform around the n_1 axis is defined as rolling motion α , and the rotation around the n_2 axis is defined as pitching motion β . The attitude signal of the platform is obtained by the inclination sensor arranged on the moving platform. In Figures 10 and 11, the tracking curve of compound impedance control can reproduce the shape of the command curve, while the PID control shows obvious errors when the command speed sharply changes.

In Figure 12, the trajectory tracking curve of the manipulator in the pitch-roll motion plane is given with compound impedance and PID control. The tracking command is the synthetic motion of the moving platform in the pitch-roll motion plane shown in Figures 9 and 10. In Figure 12, the platform with compound impedance control shows better tracking ability than that with PID control.

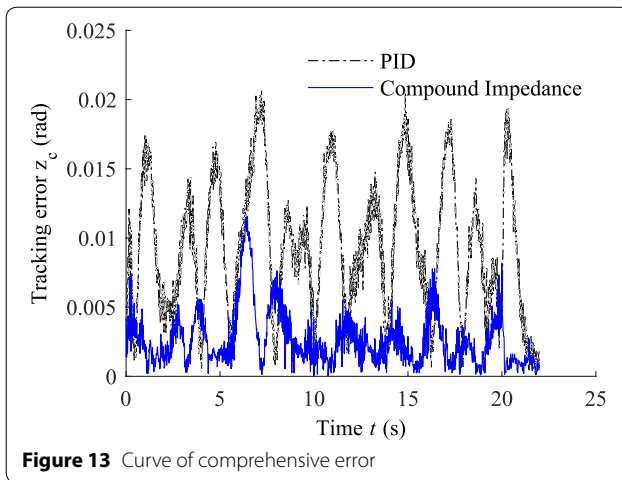


Figure 13 Curve of comprehensive error

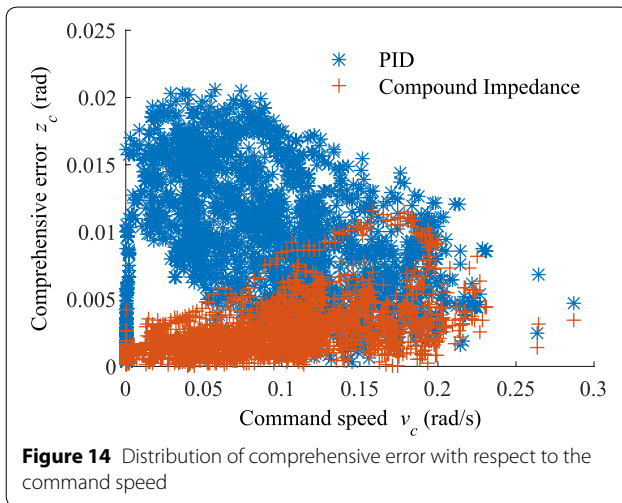


Figure 14 Distribution of comprehensive error with respect to the command speed

The trajectory tracking performance of the parallel manipulator can be evaluated by the concept of comprehensive error [41]. In the pitch-roll plane, the trajectory error is defined as

$$z_c = \sqrt{E_p^2 + E_R^2}, \quad (52)$$

where E_p is the pitch trajectory tracking error of the moving platform, and E_R is the roll trajectory tracking error.

Figure 13 shows the variation of synthetic error with respect to time. From Figure 13, the PID control error shows a continuous fluctuation trend with a peak of approximately 0.02 rad and an average of approximately 0.01 rad. Whereas, the compound impedance control error is maintained at a low level overall, with a peak of 0.01 rad and an average of approximately 0.005 rad. Jouni Mattila [31] adopted the ratio of tracking error and motion speed to evaluate the control accuracy level of the mechanism. Figure 14 shows the distribution of the

command velocity of the comprehensive trajectory error with different control methods. The comprehensive trajectory error definition is shown in Eq. (52), and the command speed is defined as:

$$v_c = \sqrt{\hat{v}_P^2 + \hat{v}_R^2}, \quad (53)$$

where \hat{v}_P is the command speed of the moving platform in pitch motion; \hat{v}_R is the roll command speed in roll motion.

From Figure 14, the compound impedance control error increases gradually with the command speed in the low-speed interval with the rate of 0.1 s. With further increasing command speed, the tracking error is stable at 0.005 rad. The PID control error fluctuates at 0–0.02 rad.

6 Conclusions

- (1) The trajectory tracking control of a parallel 3-DOF manipulator is studied. The kinematics and dynamics model of the 3-DOF 3UPS/S mechanism as well as the dynamics model of the hydraulic servo system are established. Through the singular perturbation analysis, a force sensor-less hydraulic force generator is obtained, and the exponential stability of the boundary layer model of the singular system is demonstrated.
- (2) A compound impedance control strategy for trajectory tracking of the hydraulic parallel manipulator is proposed. The control strategy is divided into the inner loop and outer loop. The inner loop controls the impedance of each actuator in the joint space, and the outer loop controls the impedance of the entire manipulator in the task space to compensate for the coupling of the actuators. The experimental results show that the compound impedance control has better trajectory tracking ability than that of the well-tuned PID controller.
- (3) The proposed compound impedance control does not require force or pressure sensors and has a low dependence on the accuracy of the modeling. Compared with other advanced control methods, the compound impedance control has higher control accuracy and provides a novel framework for dealing with the highly coupling and nonlinear dynamics of hydraulic parallel manipulators.

Acknowledgements

Not applicable.

Authors' Contributions

LZ was in charge of the whole trial; LW wrote the manuscript; SC and CM assisted with sampling and laboratory analyses. All authors read and approved the final manuscript.

Authors' Information

Lihang Wang, born in 1989. He received his PhD degrees from *Yanshan University, China*, in 2019. His PhD work was in the field of hydraulic servo control system for parallel mechanism.

Shaofei Cui, born in 1993, is a master candidate majoring in mechanical engineering at *Yanshan University, China*. His research interests are fluid transmission and control.

Chong Ma, born in 1994, is a master candidate majoring in mechanical engineering at *Yanshan University, China*. His research interests are fluid transmission and control.

Lijie Zhang, born in 1969, is currently a professor at *College of Mechanical Engineering, Yanshan University, China*. He received his PhD degree in 2006 from *Yanshan University, China*. His research interests include hydraulic system control, hydraulic components reliability and robot control.

Funding

Supported by National Natural Science Foundation of China (Grant No. 51875499).

Competing Interests

The authors declare no competing financial interests.

Author Details

¹ Hebei Key Laboratory of Heavy Machinery Fluid Power Transmission and Control, Yanshan University, Qinhuangdao 066004, China. ² Key Laboratory of Advanced Forging & Stamping Technology and Science, Ministry of Education of China, Yanshan University, Qinhuangdao 066004, China.

Appendix

In this Appendix, the detailed expressions for the symbols in Eq. (8) are given as follows:

$$\begin{aligned}
 \mathbf{F}_L &= (F_x \ F_y \ F_z) \begin{bmatrix} \mathbf{n}_1 \\ \mathbf{n}_2 \\ \mathbf{n}_3 \end{bmatrix}, \\
 \mathbf{T}_L &= (T_x \ T_y \ T_z) \begin{bmatrix} \mathbf{n}_1 \\ \mathbf{n}_2 \\ \mathbf{n}_3 \end{bmatrix},
 \end{aligned}
 \tag{A2}$$

where \mathbf{G}_{W_u} , $\mathbf{G}_{L_u}^i$, $\mathbf{G}_{L_d}^i$ are the gravity of the moving platform and the i th driving branch, given below:

$$\begin{aligned}
 \mathbf{G}_{W_u} &= (0, 0, -m_A g) \begin{bmatrix} \mathbf{n}_1 \\ \mathbf{n}_2 \\ \mathbf{n}_3 \end{bmatrix}, \quad \mathbf{G}_{L_u}^i = (0, 0, -m_{L_u}^i g) \begin{bmatrix} \mathbf{n}_1 \\ \mathbf{n}_2 \\ \mathbf{n}_3 \end{bmatrix}, \\
 \mathbf{G}_{L_d}^i &= (0, 0, -m_{L_d}^i g) \begin{bmatrix} \mathbf{n}_1 \\ \mathbf{n}_2 \\ \mathbf{n}_3 \end{bmatrix}.
 \end{aligned}
 \tag{A3}$$

Here, $\mathbf{v}_r^{W_u^*}$ denotes the partial velocity of the mass center of the moving platform; $\boldsymbol{\omega}_r^{W_u}$ denotes the partial angular velocity of the moving platform; $\boldsymbol{\omega}_r^{L_i}$ denotes the partial angular velocity of the i th driving branch; $\mathbf{v}_r^{L_u^*}$ denotes the partial velocity of the mass center of the i th upper driving branch, and $\mathbf{v}_r^{L_d^*}$ denotes the partial

$$\mathbf{T}(\mathbf{q}, \mathbf{F}_L, \mathbf{T}_L, \mathbf{G}) = \begin{bmatrix} (\mathbf{F}_L + \mathbf{G}^{W_u}) \cdot \mathbf{v}_1^{W_u^*} + \mathbf{T}_L \cdot \boldsymbol{\omega}_1^{W_u} + \sum \left(\mathbf{G}_{L_u}^i \cdot \mathbf{v}_1^{L_u^*} + \mathbf{G}_{L_d}^i \cdot \mathbf{v}_1^{L_d^*} \right) \\ (\mathbf{F}_L + \mathbf{G}^{W_u}) \cdot \mathbf{v}_2^{W_u^*} + \mathbf{T}_L \cdot \boldsymbol{\omega}_2^{W_u} + \sum \left(\mathbf{G}_{L_u}^i \cdot \mathbf{v}_2^{L_u^*} + \mathbf{G}_{L_d}^i \cdot \mathbf{v}_2^{L_d^*} \right) \\ (\mathbf{F}_L + \mathbf{G}^{W_u}) \cdot \mathbf{v}_3^{W_u^*} + \mathbf{T}_L \cdot \boldsymbol{\omega}_3^{W_u} + \sum \left(\mathbf{G}_{L_u}^i \cdot \mathbf{v}_3^{L_u^*} + \mathbf{G}_{L_d}^i \cdot \mathbf{v}_3^{L_d^*} \right) \end{bmatrix}.
 \tag{A1}$$

Here, \mathbf{F}_L and \mathbf{T}_L are the load force and moment of the moving platform, respectively, given by velocity of the mass center of the i th lower driving branch ($r = 1, 2, 3$):

$$\mathbf{M}(\mathbf{q}) = \begin{bmatrix} \mathbf{s}_1 \cdot \left(\mathbf{v}_1^{L_u^*} - \mathbf{v}_1^{L_d^*} \right) & \mathbf{s}_2 \cdot \left(\mathbf{v}_1^{L_u^*} - \mathbf{v}_1^{L_d^*} \right) & \mathbf{s}_3 \cdot \left(\mathbf{v}_1^{L_u^*} - \mathbf{v}_1^{L_d^*} \right) \\ \mathbf{s}_1 \cdot \left(\mathbf{v}_2^{L_u^*} - \mathbf{v}_2^{L_d^*} \right) & \mathbf{s}_2 \cdot \left(\mathbf{v}_2^{L_u^*} - \mathbf{v}_2^{L_d^*} \right) & \mathbf{s}_3 \cdot \left(\mathbf{v}_2^{L_u^*} - \mathbf{v}_2^{L_d^*} \right) \\ \mathbf{s}_1 \cdot \left(\mathbf{v}_3^{L_u^*} - \mathbf{v}_3^{L_d^*} \right) & \mathbf{s}_2 \cdot \left(\mathbf{v}_3^{L_u^*} - \mathbf{v}_3^{L_d^*} \right) & \mathbf{s}_3 \cdot \left(\mathbf{v}_3^{L_u^*} - \mathbf{v}_3^{L_d^*} \right) \end{bmatrix}.
 \tag{A4}$$

Here, s_i denotes the unit vector of the i th driving branch.

$$s_i = \frac{r^{B_i A_i}}{|r^{B_i A_i}|}, \tag{A5}$$

where $a^{L_i^*}$ denotes the acceleration of the mass center of the i th upper driving branch; α^{L_i} denotes the angular acceleration of the i th upper driving branch; ω^{L_i} denotes the angular velocity of the i th upper driving branch, and

$$F^*(q, \dot{q}, \ddot{q}) = \begin{bmatrix} (R^*)_{W_u} \cdot v_1^{W_u^*} + (T^*)_{W_u} \cdot \omega_1^{W_u} + \sum_i \left[(R^*)_{L_u^i} \cdot v_1^{L_u^i^*} + (T^*)_{L_u^i} \cdot \omega_1^{L_i} \right] + \\ \sum_i \left[(R^*)_{L_d^i} \cdot v_1^{L_d^i^*} + (T^*)_{L_d^i} \cdot \omega_1^{L_i} \right] \\ (R^*)_{W_u} \cdot v_2^{W_u^*} + (T^*)_{W_u} \cdot \omega_2^{W_u} + \sum_i \left[(R^*)_{L_u^i} \cdot v_2^{L_u^i^*} + (T^*)_{L_u^i} \cdot \omega_2^{L_i} \right] + \\ \sum_i \left[(R^*)_{L_d^i} \cdot v_2^{L_d^i^*} + (T^*)_{L_d^i} \cdot \omega_2^{L_i} \right] \\ (R^*)_{W_u} \cdot v_3^{W_u^*} + (T^*)_{W_u} \cdot \omega_3^{W_u} + \sum_i \left[(R^*)_{L_u^i} \cdot v_3^{L_u^i^*} + (T^*)_{L_u^i} \cdot \omega_3^{L_i} \right] + \\ \sum_i \left[(R^*)_{L_d^i} \cdot v_3^{L_d^i^*} + (T^*)_{L_d^i} \cdot \omega_3^{L_i} \right] \end{bmatrix}. \tag{A6}$$

For moving platform W_u , the generalized inertial force and generalized moment of inertia are respectively expressed as

$$\begin{aligned} (R^*)_{W_u} &= -a^{W_u^*} m_{W_u}, \\ (T^*)_{W_u} &= -\alpha^{W_u} \cdot I^{W_u} - \omega^{W_u} \times I^{W_u} \cdot \omega^{W_u}, \end{aligned} \tag{A7}$$

where $a^{W_u^*}$ denotes the acceleration of the mass center of the moving platform; α^{W_u} denotes the angular acceleration of the moving platform; ω^{W_u} denotes the angular velocity the moving platform, and I^{W_u} denotes the central inertia dyadic of the moving platform.

For the i th upper driving branch L_u^i , the generalized inertial force and generalized moment of inertia are respectively expressed as

$$\begin{aligned} (R^*)_{L_u^i} &= -a^{L_u^i^*} m_{L_u^i}, \\ (T^*)_{L_u^i} &= -\alpha^{L_u^i} \cdot I^{L_u^i} - \omega^{L_u^i} \times \left(\omega^{L_u^i} \cdot I^{L_u^i} \right), \end{aligned} \tag{A8}$$

I^{W_u} denotes the central inertia dyadic of the i th upper driving branch.

The relationship between the motion of the moving platform and generalized velocity can be obtained as follows:

$$\begin{cases} \omega^{W_u} = u_1 n_1 + u_2 n_2 + u_3 n_3, \\ \alpha^{W_u} = \dot{u}_1 n_1 + \dot{u}_2 n_2 + \dot{u}_3 n_3, \\ v^{W_u^*} = \omega^{W_u} \times r^{PW_u^*}, \\ a^{W_u^*} = \omega^{W_u} \times \left(\omega^{W_u} \times r^{PW_u^*} \right) + \alpha^{W_u} \times r^{PW_u^*}. \end{cases} \tag{A9}$$

For the i th driving branch, the relationship can be obtained by

$$\begin{cases} \omega^{L_i} = s_i \times \left(\omega^{W_u} \times r^{PA_i} \right) / \left(s_i \cdot v^{A_i} \right), \\ \alpha^{L_i} = \left(s_i \times a^{A_i} - 2\dot{L}_i \omega^{L_i} \right) / \left(s_i \cdot v^{A_i} \right), \\ v^{L_u^i^*} = v^{A_i} + \omega^{L_i} \times r^{A_i L_u^i^*} \\ a^{L_u^i^*} = a^{A_i} + e_1 s_i \left(\omega^{L_i} \right)^2 - \alpha^{L_i} \times e_1 s_i, \\ v^{L_d^i^*} = \omega^{L_i} \times r^{B_i L_d^i^*}, \\ a^{L_d^i^*} = a^{B_i} + \omega^{L_i} \times \left(\omega^{L_i} \times r^{B_i L_d^i^*} \right) + \alpha^{L_i} \times r^{B_i L_d^i^*}, \end{cases} \tag{A10}$$

Table 1 Partial velocity and partial angular velocity of the components in 3UPS/S

Component	Partial velocity	Partial velocity	Subscript range
Moving platform W_u	$\omega_r^{W_u} = \omega^{W_u} _{E_v=E_r}$	$v_r^{W_u^*} = v^{W_u^*} _{E_v=E_r}$	$r = 1, \dots, 3$
driving branch L_i	$\omega_r^{L_i} = \omega^{L_i} _{E_v=E_r}$	$v_r^{L_u^i^*} = v^{L_u^i^*} _{E_v=E_r}$	$r = 1, \dots, 3$
		$v_r^{L_d^i^*} = v^{L_d^i^*} _{E_v=E_r}$	$r = 1, \dots, 3$

where v^{A_i} denotes the velocity of upper joint A_i ; a^{A_i} denotes the acceleration of upper joint A_i , $a^{A_i} = \alpha^A \times r^{PA_i} + \omega^A \times \left(\omega^A \times r^{PA_i} \right)$.

The generalized velocity vectors are defined as

$$E_v \triangleq [u_1 \ u_2 \ u_3], \quad (A11)$$

and the unit vector is as follows:

$$\begin{aligned} E_1 &\triangleq [1 \ 0 \ 0], \\ E_2 &\triangleq [0 \ 1 \ 0], \\ E_3 &\triangleq [0 \ 0 \ 1]. \end{aligned} \quad (A12)$$

The partial velocities of each component are listed in Table 1.

Received: 16 July 2019 Revised: 29 June 2020 Accepted: 15 July 2020
Published online: 27 August 2020

References

- C F Yang, Q T Huang, J W Han, et al. Decoupling control for spatial six-degree-of-freedom electro-hydraulic parallel robot. *Robotics and Computer-Integrated Manufacturing*, 2012, 28(1): 14-23.
- S H Koekebakker. Coordinate reconstruction in model based control of a stewart platform. *IFAC Proceedings Volumes*, 1998, 31(27): 103-108.
- D Wang, J Wu, L P Wang, et al. A method for designing control parameters of a 3-DOF parallel tool head. *Mechatronics*, 2017: 102-113.
- J T Yao, D L Wang, D J Cai, et al. Fault-tolerant strategy and experimental study on compliance assembly of a redundant parallel six-component force sensor. *Sensors and Actuators A-Physical*, 2017: 114-124.
- M Honegger, R Brega, G Schweiter, et al. Application of a nonlinear adaptive controller to a 6 DOF parallel manipulator. *International Conference on Robotics and Automation*, San Francisco, California, 2000: 1930-1935.
- A Shukla, H Karki. Modeling simulation & control of 6-DOF parallel Manipulator using PID controller and compensator. *IFAC Proceedings Volumes*, 2014, 47(1): 421-428.
- P S Londhe, Y Singh, M Santhakumar, et al. Robust nonlinear PID-like fuzzy logic control of a planar parallel (2PRP-PPR) manipulator. *ISA Transactions*, 2016: 218-232.
- H Cheng, Y K Yiu, Z X Li, et al. Dynamics and control of redundantly actuated parallel manipulators. *IEEE/ASME Transactions on Mechatronics*, 2003, 8(4): 483-491.
- A Codourey. Dynamic modeling of parallel robots for computed-torque control implementation. *The International Journal of Robotics Research*, 1998, 17(12): 1325-1336.
- H Abdellatif, B Heimann. Advanced model-based control of a 6-DOF hexapod robot: a case study. *IEEE/ASME Transactions on Mechatronics*, 2010, 15(2): 269-279.
- J S Wang, J Wu, L P Wang, et al. Dynamic feed-forward control of a parallel kinematic machine. *Mechatronics*, 2009, 19(3): 313-324.
- W W Shang, S Cong, Y Ge, et al. Adaptive computed torque control for a parallel manipulator with redundant actuation. *Robotica*, 2012, 30(3): 457-466.
- L Ren, J K Mills, D Sun, et al. Experimental comparison of control approaches on trajectory tracking control of a 3-DOF parallel robot. *IEEE Transactions on Control Systems and Technology*, 2007, 15(5): 982-988.
- H S Kim, Y M Cho, K Lee, et al. Robust nonlinear task space control for 6 DOF parallel manipulator. *Automatica*, 2005, 41(9): 1591-1600.
- D H Kim, J Y Kang, K Lee, et al. Robust tracking control design for a 6 DOF parallel manipulator. *Journal of Robotic Systems*, 2000, 17(10): 527-547.
- T D Le, H J Kang, Y S Suh, et al. An online self-gain tuning method using neural networks for nonlinear PD computed torque controller of a 2-DOF parallel manipulator. *Neurocomputing*, 2013: 53-61.
- C F Yang, Q T Huang, J W Han, et al. Computed force and velocity control for spatial multi-DOF electro-hydraulic parallel manipulator. *Mechatronics*, 2012, 22(6): 715-722.
- J Cazalilla, M Valles, V Mata, et al. Adaptive control of a 3-DOF parallel manipulator considering payload handling and relevant parameter models. *Robotics and Computer-integrated Manufacturing*, 2014, 30(5): 468-477.
- Y M Li, Q S Xu. Dynamic modeling and robust control of a 3-PRC translational parallel kinematic machine. *Robotics and Computer-integrated Manufacturing*, 2009, 25(3): 630-640.
- H T Liu, X H Tian, Wang G, et al. Finite-time Hinf control for high-precision tracking in robotic manipulators using backstepping control. *IEEE Transactions on Industrial Electronics*, 2016, 63(9): 5501-5513.
- Y Singh, V Vinoth, Y R Kiran, et al. Inverse dynamics and control of a 3-DOF planar parallel (U-shaped 3-PPR) manipulator. *Robotics and Computer-Integrated Manufacturing*, 2015: 164-179.
- N Hogan. Impedance control: An approach to manipulation: Part I—Theory. *Journal of Dynamic Systems Measurement and Control-Transactions of the ASME*, 1985, 107(1): 1-7.
- H Sadjadian, H D Taghiradf. Impedance control of the hydraulic shoulder a 3-DOF parallel manipulator. *Robotics and Biomimetics*, 2006: 526-531.
- H Z Arabshahi, A B Novinzadeh. Impedance control of the 3RPS parallel manipulator. *International Conference on Robotics and Mechatronics*, Bali, Indonesia, 2014: 486-492.
- A K Ghosh. Dynamics and robust control of robotic systems: a bond graph approach. Kharagpur: *Indian Institute of Technology*, 1990.
- P M Pathak, A Mukherjee, A Dasgupta, et al. Impedance control of space robots using passive degrees of freedom in controller domain. *Journal of Dynamic Systems Measurement and Control-Transactions of the ASME*, 2005, 127(4): 564-578.
- W Ye, Q C Li. Type synthesis of lower mobility parallel mechanisms: A review. *Chinese Journal of Mechanical Engineering*, 2019, 32(1): 1-11.
- Q Liu, J L Xiao, X Yang, et al. An iterative tuning approach for feedforward control of parallel manipulators by considering joint couplings. *Mechanism and Machine Theory*, 2019: 159-169.
- S Mohan. Error analysis and control scheme for the error correction in trajectory-tracking of a planar 2PRP-PPR parallel manipulator. *Mechatronics*, 2017: 70-83.
- L Angel, J Viola. Fractional order PID for tracking control of a parallel robotic manipulator type delta. *ISA Transactions*, 2018: 172-188.
- J Mattila, J Koivumaki, D G Caldwell, et al. A survey on control of hydraulic robotic manipulators with projection to future trends. *IEEE-ASME Transactions on Mechatronics*, 2017, 22(2): 669-680.
- W H Ding, H Deng, Y M Xia, et al. Tracking control of electro-hydraulic servo multi-closed-chain mechanisms with the use of an approximate nonlinear internal model. *Control Engineering Practice*, 2017: 225-241.
- H B Guo, Y G Liu, G R Liu, et al. Cascade control of a hydraulically driven 6-DOF parallel robot manipulator based on a sliding mode. *Control Engineering Practice*, 2008, 16(9): 1055-1068.
- S H Chen, L C Fu. Observer-based backstepping control of a 6-dof parallel hydraulic manipulator. *Control Engineering Practice*, 2015, 36(36): 100-112.
- J Koivumaki, J Mattila. Stability-guaranteed force-sensorless contact force/motion control of heavy-duty hydraulic manipulators. *IEEE Transactions on Robotics*, 2015, 31(4): 918-935.
- Y Z Huang, D M Pool, O Stroosma, et al. Long-stroke hydraulic robot motion control with incremental nonlinear dynamic inversion. *IEEE/ASME Transactions on Mechatronics*, 2019, 24(1): 304-314.
- S Yoo, W Lee, W K Chung, et al. Impedance control of hydraulic actuation systems with inherent backdrivability. *IEEE/ASME Transactions on Mechatronics*, 2019, 24(5): 1921-1930.
- Hassan K Khalil. *Nonlinear systems*. 3rd ed. Prentice Hall, 2001.
- C W Wang, L Quan, S J Zhang, et al. Reduced-order model based active disturbance rejection control of hydraulic servo system with singular value perturbation theory. *ISA Transactions*, 2017, 67: 455-465.
- A Zubizarreta, M Larrea, E Irigoyen, et al. Real time direct kinematic problem computation of the 3PRS robot using neural networks. *Neurocomputing*, 2018, 271: 104-114.
- J H Chin, Y Sun, Y M Cheng, et al. Force computation and continuous path tracking for hydraulic parallel manipulators. *Control Engineering Practice*, 2008, 16(6): 697-709.